Electronic Supplementary Material (ESI) for Lab on a Chip.
This journal is © The Royal Society of Chemistry 2014

Supplementary information Resonance-enhanced microfluidic impedance cytometer for detection of single bacteria

Niels Haandbæk[*a], Oliver With[a], Sebastian C. Bürgel[a], Flavio Heer[b] and Andreas Hierlemann[a]

Full electrical equivalent circuit model

The following figure illustrates the full electrical equivalent circuit model that was fitted to the measured magnitude and phase response of the system. The lumped-element model of the inductor was taken from the manufactures documentation (http://www.coilcraft.com/pdfs/spice_1812CS.pdf). R_{var} models the skin effect and is frequency dependent. Its value is given by $R_{var} = k\sqrt{f}$, where f is the frequency in Hz and $k = 1.8\times10^{-3}$ for the chosen inductor component. The values of the other components are: $C1$ = 122 fF, $R1$ = 85 Ω and $R2$ = 5.4 Ω.

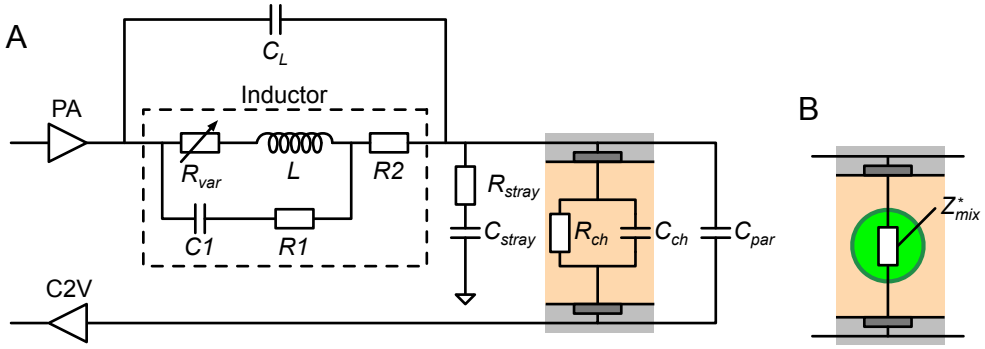

Supplementary figure 1: (A) Full electrical equivalent circuit model with component values adjusted to fit the measured magnitude and phase response of the system. (B) The channel is modeled with a complex impedance, Z^*_{mix}, when a particle or cell is present between the electrodes.

The channel is modeled by the complex impedance, Z^*_{mix}, when a particle or cell is present between the electrodes. The complex impedance is given by the equations presented by Sun et al.[1]:

$$Z^*_{mix} = \frac{1}{j2\pi f \varepsilon^*_{mix} G_f} \tag{1}$$

Here, $j = \sqrt{-1}$, f is the frequency, $\mathcal{E}^*_{mix}$ the complex permittivity of the channel with a cell or particle present and G_f the geometric factor of the system. The dimensions of the microfluidic channel in terms of width, l, height, h, and the width of the electrodes, w, determine the geometric factor:

$$G_f = \frac{wl}{h} \tag{2}$$

The complex permittivity of the channel with particle is given by

$$\varepsilon^*_{mix} = \varepsilon^*_m \frac{1 + 2\Phi F^*_{CM}}{1 - \Phi F^*_{CM}} \tag{3}$$

where Φ is the volume fraction of the particle and F^*_{CM} denotes the complex Clausius-Mosotti factor:

$$F^*_{CM} = \frac{\varepsilon^*_p - \varepsilon^*_m}{\varepsilon^*_p + 2\varepsilon^*_m} \tag{4}$$

Finally, the complex permittivity of the suspending medium, $\mathcal{E}^*_m$, as well as that of the cell or particle, $\mathcal{E}^*_p$, is given by

$$\varepsilon^* = \varepsilon_0 \varepsilon_r - j\frac{\sigma}{2\pi f} \tag{5}$$

where ε_r is the dielectric constant and σ the conductivity of the corresponding material.

Sensitivity of phase to changes in channel capacitance and resistance

Supplementary figure 2 shows that the measured change in phase of the polystyrene beads is linearly related to the corresponding change in channel capacitance. The change in channel capacitance was computed based on the equivalent electrical circuit model described above.

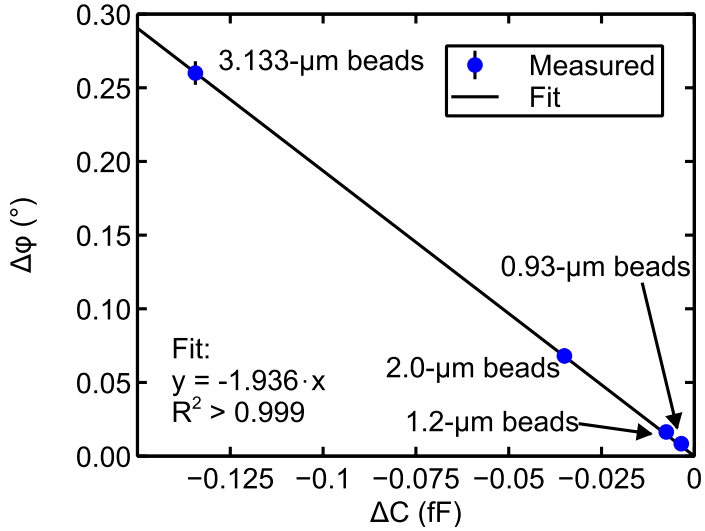

Supplementary figure 2: Comparison of the measured change in phase (Δφ) as a function of the computed change in channel capacitance (ΔC) of the beads used in this study.

Supplementary figure 3A compares the sensitivity of the system to changes in channel capacitance at the two measurement frequencies. As seen from the figure, the system is more sensitive to changes in phase at the primary measurement frequency of 89.2 MHz, which is close to resonance, compared to the secondary frequency of 87.2 MHz. It is also clear that the change in phase is directly proportional to the change in channel capacitance. A similar plot is shown for changes in channel resistance in Supplementary figure 3B. In contrast to Supplementary figure 3A, the sensitivity is higher at the secondary frequency compared to the primary frequency. Furthermore, as can be seen from the fitting functions, the change in phase is inversely proportional to the change in channel resistance.

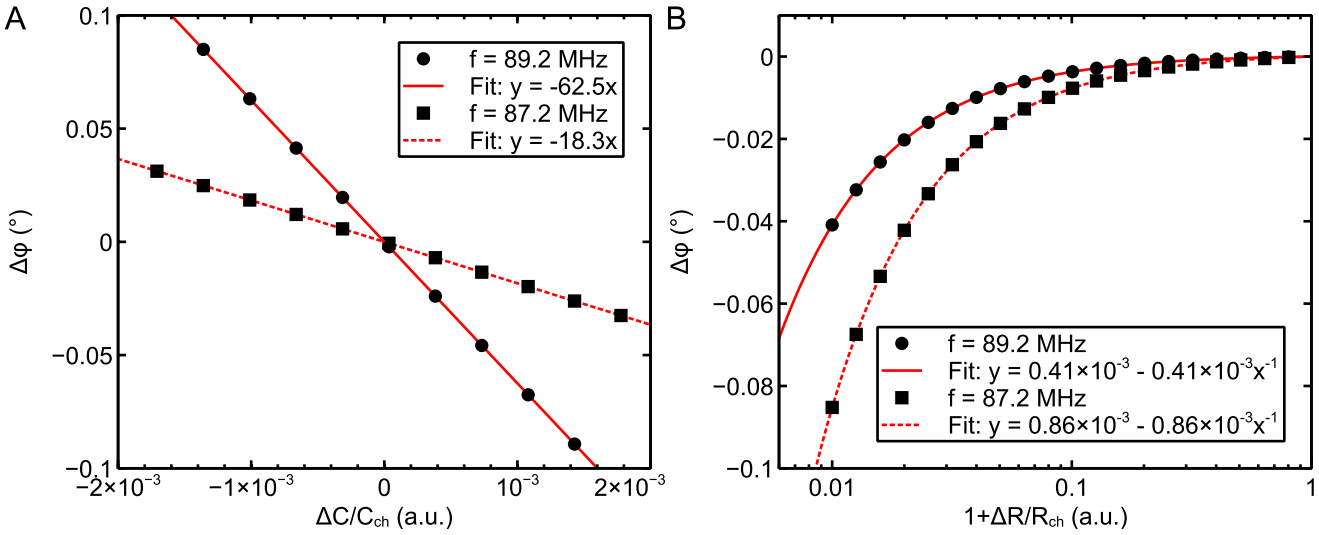

Supplementary figure 3: (A) Illustration of the sensitivity of the system to changes in the channel capacitance at the two measurement frequencies computed based on the electrical equivalent circuit model. The capacitive change has been normalized to the channel capacitance of 29.0 fF. The sensitivity of 2.2°/fF at 89.2 MHz and 0.63°/fF at 87.2 MHz can be computed based on the slope of the linear fits and the channel capacitance of 29.0 fF. (B) Illustration of the sensitivity of the system to changes in the channel resistance at the two measurement frequencies computed based on the electrical equivalent circuit model. The resistive change has been normalized to the channel resistance of 4.44 GΩ and shifted by +1 in order to allow the x-scale to be represented logarithmically. The system is more sensitive to resistive changes at the lower measurement frequency.

The curves shown in Supplementary figure 3 can also be used to compute the change in channel capacitance and resistance as a function of the change in phase measured at the primary and secondary frequency using the following expressions. First, the total change in phase is approximated as the sum of the change due to the capacitive and resistive parts:

$$\Delta\varphi \approx \Delta\varphi_C + \Delta\varphi_R \tag{6}$$

By inserting the expressions for the capacitive and resistive change shown in Supplementary figure 3 into equation 6, a system of two equations with two unknowns can be formed:

$$\Delta\varphi_{89.2MHz} = -62.5\,\Delta C/C_{ch} + 0.41\times10^{-3} - 0.41\times10^{-3}(1 + \Delta R/R_{ch}) \tag{7}$$

$$\Delta\varphi_{87.2MHz} = -18.3\,\Delta C/C_{ch} + 0.86\times10^{-3} - 0.86\times10^{-3}(1 + \Delta R/R_{ch}) \tag{8}$$

The expressions can then be solved to give the change in channel capacitance, ΔC, and resistance, ΔR, as a function of the measured change in phase at the primary, $\Delta\varphi_{89.2MHz}$, and secondary, $\Delta\varphi_{87.2MHz}$, frequency.

Optical determination of *E. coli* and *B. subtilis* size

Prior to imaging both bacterial strains were stained using a standard Gram staining kit (Becton Dickinson AG, Switzerland), by following the protocol specified by the manufacturer. The images were recorded on a Nikon Optiphot 200 (Nikon AG, Switzerland) microscope at a total magnification of ×50 using a Leica DFC 280 camera (Leica Microsystems Gmbh, Germany). The images were analyzed using MATLAB (MathWorks, Inc., USA) to detect and measure the size of the individual cells. Example images and the resulting distribution of volumes of cells detected in all recorded images are illustrated in the following figure.

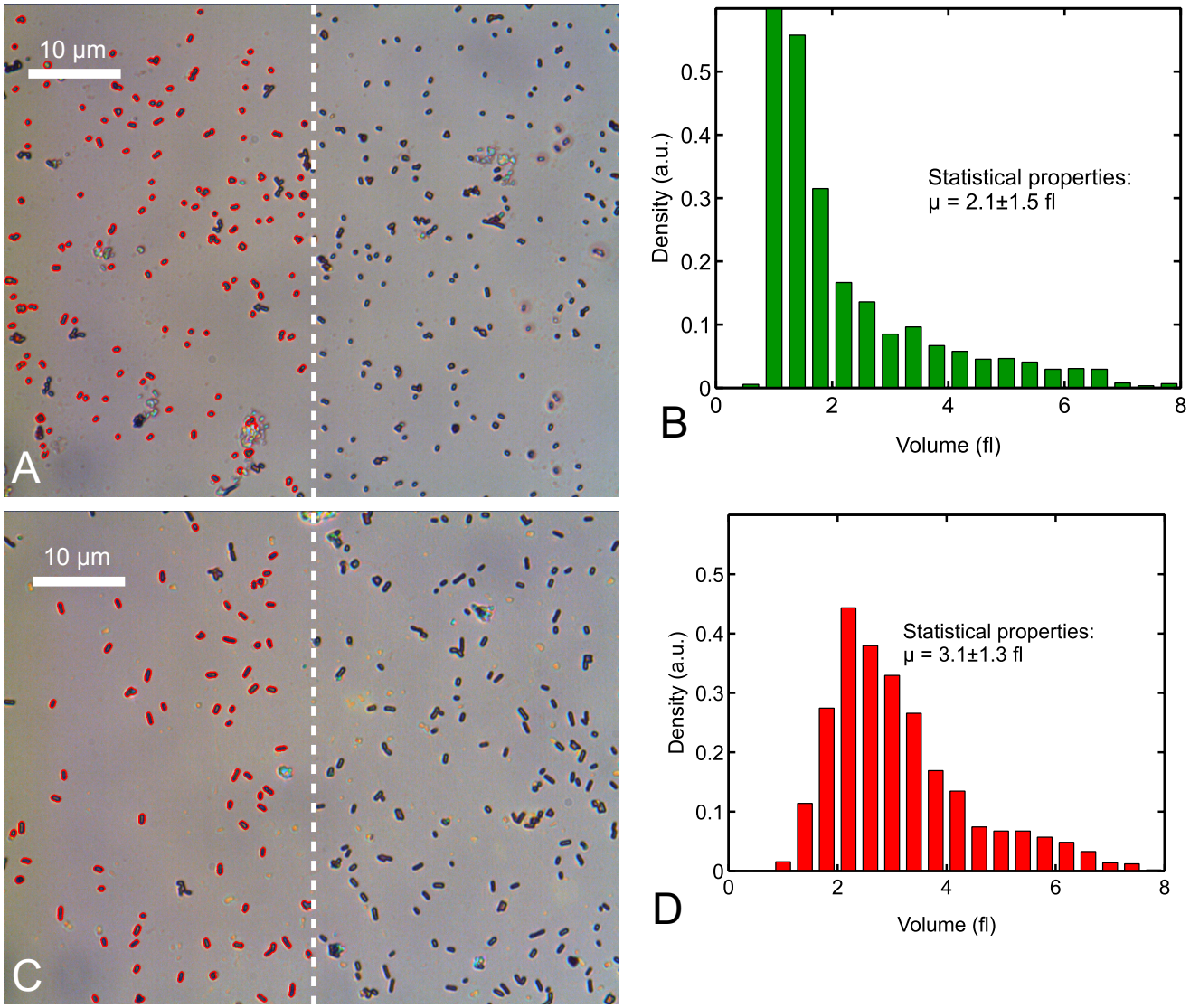

Supplementary figure 4: (A) Bright-field micrograph of E. coli after adjustment of tone, color and contrast. The outline of the cells, which is used for the calculation of width, length and volume, is shown in red on the left half of the image. (B) Corresponding histogram of cell lengths of 2,210 E. coli cells. (C) Bright-field micrograph of B. subtilis *after adjustment of tone, color and contrast. Again, the outlines of the detected cells are shown on the left half of the image. (D) Corresponding histogram of cell lengths of 3,105* B. subtilis *cells. The arithmetic mean and standard deviation of the histograms are indicated on the figures.*

The cell volume was computed as

$$V = (l - d)\pi\left(\frac{d}{2}\right)^2 + \frac{4}{3}\pi\left(\frac{d}{2}\right)^3 \quad \textbf{(1)}$$

where l is the cell length and d the diameter. The cell length was found to be 1.9±0.6 µm for the *E. coli* and 2.3±0.5 µm for the *B. subtilis* cells. The cell diameter was found to be 1.3±0.2 µm and 1.4±0.2 µm, respectively.

Sensitivity as a function of medium conductivity

Supplementary figure 5 shows the performance of the resonator as a function of medium conductivity. Supplementary figure 5A shows the magnitude and phase of the measured voltage as the medium conductivity is varied between 5.5 µS/m and 300 mS/m. The curves have been computed based on the full electrical equivalent circuit model described previously. As can be seen from the figure, an increase in medium conductivity leads to a lower amplitude of the resonance peak. Furthermore, the slope of the phase curve at resonance also decreases with increasing medium conductivity. The

combination of these two effects leads to a reduction in the quality factor of the resonator with increasing medium conductivity, as illustrated in Supplementary figure 5B.

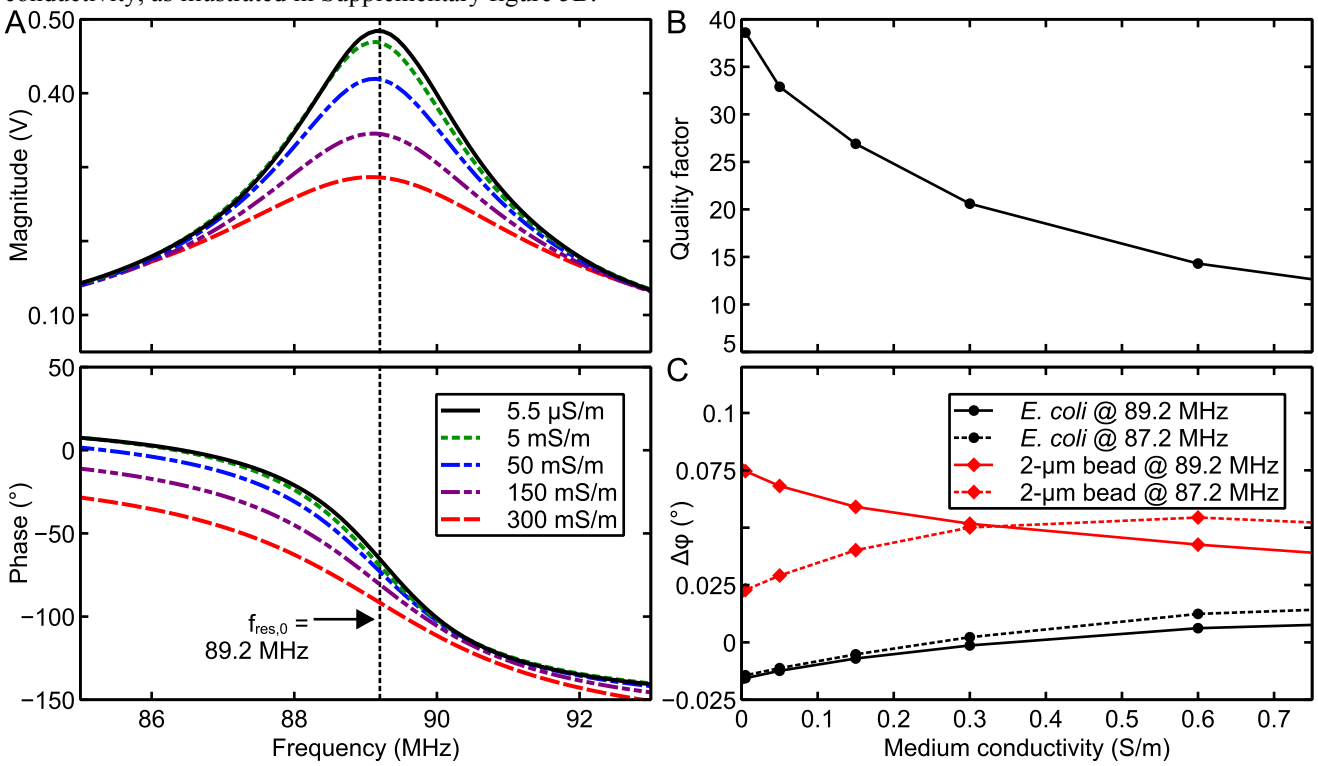

Supplementary figure 5: (A) Magnitude and phase response of the series resonance circuit as a function of the frequency and medium conductivity. (B) Resulting quality factor of the resonator, computed as $Q = f_{res,0}/\Delta f$*, where* Δf *is the 3 dB bandwidth of the resonator. (C) Expected phase shift of* E. coli *and 2-µm bead as a function of medium conductivity and frequency.*

The efficacy of the presented resonance-enhancement principle is highly dependent on the slope of the phase curve at resonance: a larger slope results in a system with higher sensitivity. Therefore, the highest sensitivity is achieved at the lowest possible medium conductivity. As an example, the sensitivity is reduced by approximately 25% when a medium conductivity of 50 mS/m is used. We estimate that this is the maximum medium conductivity that can be used with the presented resonator, which still allows detection of bacterial sized objects.

Supplementary figure 5C shows the expected phase shift of an *E. coli* cell and a 2-µm bead as a function of the medium conductivity. The values were also calculated based on the electrical equivalent circuit model. As can be seen from the figure, the cells only give rise to a phase shift if there is a difference in conductivity between the medium and the cytoplasm. Furthermore, the polarity of the phase shift depends on the relationship between medium conductivity and cytoplasm conductivity: negative when the medium is less conductive than the cytoplasm and positive when the medium is more conductive. The advantage of the presented system, which allowed the cells to be discriminated from the beads based only on the polarity of the phase shift, is, therefore, lost at higher medium conductivities.

Influence of DEP focusing on phase shift

The use of DEP focusing may cause concern regarding buildup of surface charge on the cells, which could influence their electrical properties. Supplementary figure 6 shows the results of measurements with and without the DEP field activated. The geometric mean of the phase shift of the cells is −7.4° when the DEP focusing is on, compared to −6.7° when the DEP focusing is off. The 10% larger phase shift measured with DEP focusing activated, may be explained by the fact that the cells are focused in the center of the channel, which results in a slightly improved signal-to-noise ratio.

The effect of the DEP focusing is more pronounced when the results of the beads are observed. Here, a phase shift of 42°±12° is measured when the DEP focusing is off, which corresponds to a coefficient of variation (CV) of 29%. When the DEP focusing is activated, a phase shift of 38°±4.5° is measured (CV of 12%). The drop in CV from 29% to 12% is a result of the reduced positional variation of the beads caused by the activation of the DEP focusing field.

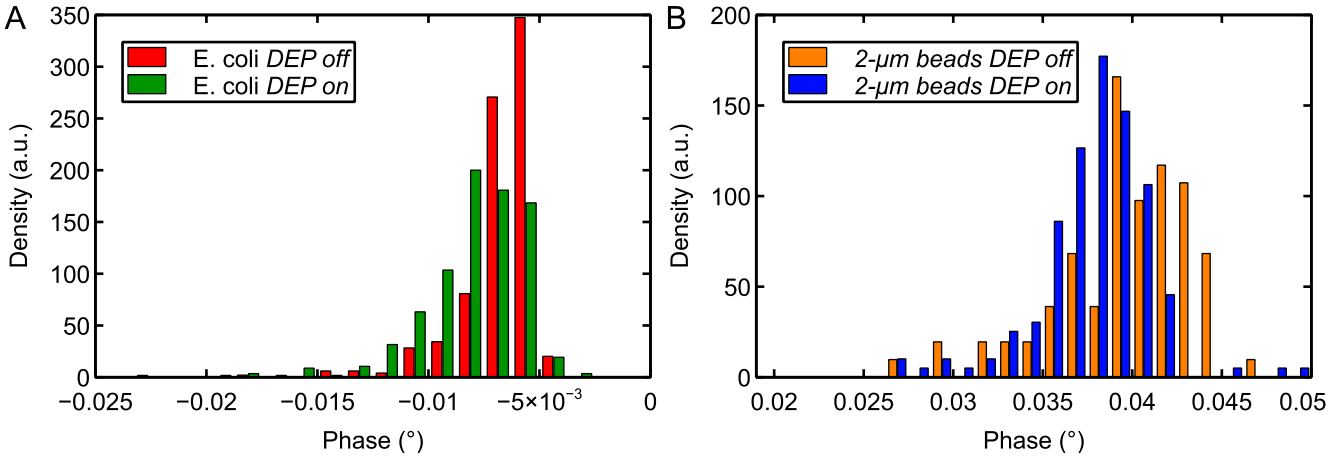

Supplementary figure 6: (A) Phase shift of E. coli *cells measured at 88.9 MHz with DEP focusing activated and deactivated. (B) Phase shift of 2-µm beads measured at 88.9 MHz with DEP focusing activated and deactivated.*

Notes

[a] ETH Zurich, Dept. of Biosystems Science and Engineering, Mattenstrasse 26, Basel, CH-4058, Switzerland. Fax: +41 61 387 3992; Tel: +41 61 387 3183; E-mail: niels.haandbaek@bsse.ethz.ch
[b] Zurich Instruments AG, Technoparkstrasse 1, Zurich, CH-8005.

References

1. T. Sun, C. Bernabini, and H. Morgan, Langmuir, 2010, 26, 3821–8.